



Selective hydrogenation of phenol to cyclohexanone by SiO₂-supported rhodium nanoparticles under mild conditions

Hongwei Zhang^a, Aijuan Han^a, Kazu Okumura^b, Lixiang Zhong^c, Shuzhou Li^c, Stephan Jaenicke^a, Gaik-Khuan Chuah^{a,*}

^a Department of Chemistry, National University of Singapore, 3 Science Drive 3, Singapore 117543, Singapore

^b Department of Applied Chemistry, School of Advanced Engineering, Kogakuin University, 2665-1 Nakano-machi Hachioji-city, 192-0015 Tokyo, Japan

^c Center for Programmable Materials, School of Materials Science and Engineering, Nanyang Technological University, Singapore 639798, Singapore

ARTICLE INFO

Article history:

Received 7 November 2017

Revised 19 April 2018

Accepted 3 June 2018

Keywords:

Rhodium

Phenol hydrogenation

Cyclohexanone

Particle size

Site specificity

Thiol-modification

ABSTRACT

A silica-supported rhodium catalyst for the selective hydrogenation of phenol to cyclohexanone under mild conditions has been developed. As the Rh concentration on the catalyst increased from 0.5 to 15 wt%, the conversion (at phenol/Rh mole ratio 100/1) dropped whereas the initial selectivity to cyclohexanone increased. The direct hydrogenation to cyclohexanol occurred in parallel with partial hydrogenation to cyclohexanone. The negative correlation between selectivity and Rh dispersion suggests that direct hydrogenation occurs at low coordination sites whereas dissociation of phenol to phenoxy followed by hydrogenation to cyclohexanone takes place at higher coordinated terrace sites. DFT calculations revealed that the activation barrier for O–H bond cleavage is lower for phenol adsorbed on a Rh(1 1 1) flat surface than on small particles. By blocking the low coordination edge and step sites through grafting with (3-mercaptopropyl)trimethoxysilane, the cyclohexanone selectivity was improved from 82 to 93% at 100% conversion. The catalyst is active at room temperature and 1 atm H₂ pressure and can be easily activated by *in-situ* reduction.

© 2018 Elsevier Inc. All rights reserved.

1. Introduction

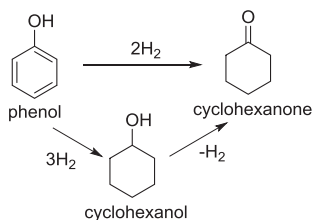
Cyclohexanone is an important intermediate in the synthesis of caprolactam for nylon-6 and adipic acid for nylon-6,6 with about 97% of the annual production being devoted for this purpose [1,2]. The balance is used as building block in the synthesis of pharmaceuticals, herbicides, insecticides and as a specialty solvent for resins and lacquers. Commercially, cyclohexanone is prepared by the catalytic oxidation of cyclohexane or via the hydrogenation of phenol in either a one- or two-step process [3]. In the two-step process, phenol is fully hydrogenated to cyclohexanol followed by an endothermic dehydrogenation step to cyclohexanone (Scheme 1). A one-step process where phenol is selectively hydrogenated to cyclohexanone is certainly preferred due to savings in costs and energy.

Phenol hydrogenation can be carried out in the gas or liquid phase [4–10]. Attaining high selectivity at elevated conversions under mild reaction conditions is a challenging catalytic problem as it is difficult to stop the reaction at cyclohexanone. The

selectivity for cyclohexanone can be influenced by a number of parameters including the type of metal [5,9–11], its particle size [12–14], and the nature of the support [7,12,14–18]. Various metals such as palladium [6,7,12,14–18], Raney nickel [19], platinum [10,20], rhodium [21–23], as well as bimetallic Pd-Mg, Pd-Ce and Au-Pd [9,24,25] are active for this reaction. In general, palladium catalysts show good selectivity to cyclohexanone although the activity is not high. Therefore, high hydrogen pressure (>5 bar), temperature (>50 °C) and phenol/Pd molar ratios of 5–20 are typically used. Liu et al reported that the activity and cyclohexanone selectivity could be enhanced to >99.9% when Pd/C was used in combination with AlCl₃ [7]. The addition of the Lewis acid was suggested to activate the benzene ring for hydrogenation while inhibiting the formed cyclohexanone. However, AlCl₃ is hygroscopic and reacts with moisture to form corrosive HCl, posing difficulties in handling and reusability. Hence, recent attention has focused on finding suitable supports that can enhance the activity and selectivity of Pd under moderate temperatures and hydrogen pressure even when water is used as the solvent. Several materials have been reported including high surface area Al₂O₃ [15] and ceria [26], hydroxyapatite [27], TiN [28], hydrophilic carbon [29], metal organic frameworks MIL-101 [14] and ZIF-67 [29], alkali

* Corresponding author.

E-mail address: chmcgk@nus.edu.sg (G.-K. Chuah).



Scheme 1. Hydrogenation of phenol.

metal-promoted TiO₂ [30], poly(N-vinyl-2-pyrrolidone) [30] and polyaniline-functionalized carbon nanotubes [31]. Notably, aqueous phase systems using palladium supported on polymeric mesoporous graphitic carbon nitride (mpg-C₃N₄) [6,32] and TiO₂-C composites [18] gave >99% selectivity to cyclohexanone at 100% conversion. Palladium nanoparticles supported on a specially designed mesostructured silica (MMT-1) was found to exhibit high phenol conversion with 98% selectivity at room temperature and atmospheric H₂ pressure [33]. Besides gaseous hydrogen, potassium formate, sodium formate and formic acid have also been used for phenol hydrogenation [34–36]. However, these alternative hydrogen sources adsorb competitively at the catalyst surface and an optimized ratio must be worked out to avoid inhibition of the reaction.

Rhodium is known for its high activity for hydrogenation of the aromatic ring under very mild conditions [22,37,38]. However, there are only a few studies on its use for phenol hydrogenation due to poor selectivity to cyclohexanone. For example, the use of carbon nanofiber-supported rhodium in supercritical CO₂ resulted in 100% phenol conversion within 0.5 h (at phenol/Rh molar ratio of 436) but the selectivity to cyclohexanone was only 43% [21]. Kempe's group reported that small rhodium nanoclusters of ~1.6–2.8 nm stabilized in a polymer-derived silicon carbonitride (SiCN) matrix formed highly active catalysts for the selective hydrogenation of phenolic compounds [39]. At 25 °C and 6 bar H₂, 99% phenol conversion was obtained in comparison to 49% and 36% for Al₂O₃- and C-supported Rh, respectively. The selectivity to cyclohexanone for the three catalysts was only 73–78%. In comparison, a high selectivity of 92% at >95% conversion was found for Rh@S-MIL-101 catalyst operating at 50 °C and 5 bar H₂ [40]. The good performance was attributed to host-guest cooperation between the rhodium nanoparticles and sulfonated MIL-101 framework as well as the presence of Cr(III) Lewis acidic sites in the support. Kuklin et al reported 100% yield of cyclohexanone using polyacrylic acid-stabilized rhodium nanoparticles modified with 20-fold excess cyclodextrin at 80 °C and 10 to 40 atm H₂ using n-hexyltriethylammonium bromide as solvent [41].

Although these results showed that selective hydrogenation to cyclohexanone could be obtained over Rh catalysts at higher temperatures and pressures, we were interested in whether the same could be achieved under ambient conditions. This work investigates if metal loading, particle size, support, and selective inhibition of certain active sites can improve the selectivity to cyclohexanone without compromising on the mild reaction conditions. Selective inhibition of the metal sites was carried out by grafting of organic functional groups with amine and thiol moieties onto the catalyst.

2. Experimental

2.1. Catalyst preparation

2.1.1. Synthesis of metal oxide-supported Rh catalysts

Rhodium was supported on the following metal oxides – SiO₂ (Merck), La₂O₃, TiO₂ (Degussa), MgO (Merck) and ZrO₂

(synthesized). For a typical preparation of 5 wt% Rh/SiO₂, 127.9 mg (0.049 mmol) RhCl₃·3H₂O, 0.95 g (15.8 mmol) SiO₂ and 20 ml deionized water were added into a 100 ml beaker. After stirring at room temperature for 3 h, the orange colored slurry was heated to almost dryness and placed overnight in an oven at 90 °C. The sample was calcined at 400 °C for 4 h in air. Samples with 0.5 to 15 wt Rh% were similarly prepared.

2.1.2. Grafted Rh catalysts

The 5 wt% Rh/SiO₂ sample was grafted with molecules of different chain length and chemical groups as shown in Table 1. The hydroxyl groups of the support react with the methoxysilane moiety to chemically bind the molecules to the surface. In a typical synthesis, 0.1 g of 5 wt% Rh/SiO₂ catalyst, (3-mercaptopropyl)trimethoxysilane (molar ratio to Rh = 2:1) and 20 ml toluene were placed in a two-necked 50 ml round bottom flask equipped with a septum port and a reflux condenser. After stirring at 110 °C for 24 h, the slurry was filtered, washed with acetone three times and dried at room temperature overnight. The samples are named as *molecule*-5 wt% Rh/SiO₂ where *molecule* represents *Amine-n*, *Glycidyl*, *Aniline*, *Thiol* and *Chloro*.

2.2. Catalyst characterization

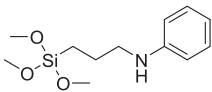
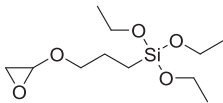
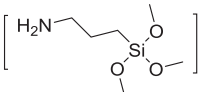
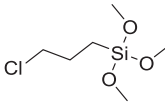
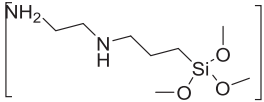
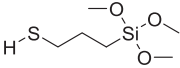
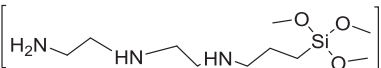
The surface area and porosity of the catalysts were determined from N₂ adsorption/desorption isotherms (Micromeritics Tristar 3000). Prior to the measurement, the sample was pretreated under a nitrogen flow at 300 °C for 5 h. Powder X-ray diffraction was performed with a Bruker D8 Advance diffractometer equipped with Cu anode, variable slits and a LynxEye XE detector. The 2θ range from 20 to 80° was measured using a step size of 0.02° and a dwell time of 1 s. Transmission electron micrographs (TEM) were obtained using a JEOL 3010 operated at 200 kV. The sample was finely ground and suspended in 2-propanol. A drop of the suspension was placed onto a carbon-coated copper grid and dried at room temperature.

X-ray photoelectron spectroscopy (XPS) was performed using a VG-Scientific ESCALAB Mark 2 spectrometer equipped with a hemispherical electron analyzer and a Mg Kα anode (1253.6 eV) operating at 300 W (15 kV × 20 mA). Wide and detailed spectra were collected in constant analyzer energy mode with a step of 1 and 0.05 eV, respectively. The analyzed area was 3.0 mm in diameter with medium magnification for samples. The binding energy of the elements was referenced to the C 1 s signal of ubiquitous carbon at 285 eV. The spectra were evaluated using a nonlinear (Shirley) background subtraction.

The elemental composition of the samples was measured by inductively coupled plasma optical emission spectroscopy (ICP-OES) using an Optima 5300 DV ICP-OES system. To dissolve the sample, about 5 mg sample was placed in a Teflon liner with 1 ml of hydrofluoric acid (40%) and heated at 98 °C for an hour, followed by the addition of a mixture of concentrated HCl (37%) and HNO₃ (69%) (volume ratio: 20:1). The sample was then placed in a microwave oven and heated at 200 °C for 2 h. The obtained solution was diluted to 10 ml before analysis.

Infrared spectroscopy for CO adsorption was performed using a Perkin Elmer Spectrum Two spectrometer. The sample was pressed into a self-supporting wafer and mounted in an evacuable quartz IR cell with CaF₂ windows. After evacuation, the sample was reduced under H₂ flow at room temperature for 1 h. The cell was evacuated to 10⁻³ mbar and CO was introduced. The sample was equilibrated in 1 atm CO for 1 h. After pumping off the gas, FTIR measurements were performed at different time intervals using a resolution of 2 cm⁻¹ and 32 scans. In order to determine the metal dispersion, pulsed CO chemisorption was carried out using a homemade temperature programmed desorption apparatus

Table 1
Nomenclature of molecules grafted on 5 wt% Rh/SiO₂.

Molecule	Name	Molecule	Name
	Aniline		Glycidyl
N-[3-(trimethoxysilyl)propyl]aniline		(3-glycidyloxypropyl)triethoxysilane	
	Amine-1		Chloro
3-aminopropyltrimethoxysilane		(3-chloropropyl)trimethoxysilane	
	Amine-2		Thiol
3-(2-aminoethylamino)propyltrimethoxysilane		(3-mercaptopropyl)trimethoxysilane	
	Amine-3		
3-[2-(2-aminoethyl amino)ethyl amino]propyltrimethoxysilane			

equipped with a quadrupole mass spectrometer. The sample was placed in a quartz reactor and pretreated in flowing H₂ at room temperature for 1 h. After flushing in 50 ml min⁻¹ He for 2 h, 50 μl pulses of CO was introduced to the sample until the CO signal reached saturation. From the total uptake of CO, the metal dispersion was calculated based on the FTIR peak areas using integrated absorption coefficients of 13, 42 and 130 cm μmol⁻¹ for linear-, bridge- and germinal-bonded CO on Rh [42]. Thermogravimetric analysis (TGA) was carried out with a TA Instruments Discovery instrument. About 10 mg of the grafted sample was kept at 100 °C for 1 h under a flow of purified air to remove physically adsorbed water before raising the temperature at 5 °C/min to 450 °C. From the weight loss, the mass of the organic component in the sample could be calculated.

Rhodium K edge (23.2 keV) XAFS data were collected at the BL01B1 station of the Japan Synchrotron Radiation Research Institute (JASRI). A Si(111) single crystal was used to obtain a monochromatic X-ray beam. The measurement was carried out in the quick mode. Ion chambers filled with Ar (100%) and N₂ (75%)/Ar (25%) were used to determine I₀ and I, respectively. The samples were pressed into self-supporting wafers. The data analysis was performed using the REX2000 Ver. 2.0.4 program (Rigaku). Fourier transformations of k³χ(k) data were performed in the k range of 30–160 nm⁻¹.

2.3. Catalytic tests

The reaction was typically carried out in a two-necked round bottom flask containing 1.5 mmol phenol (0.141 g) in 25 ml of cyclohexane at ambient temperature (25 °C). The catalyst at a Rh:phenol mole ratio of 1:100 was added. To check for mass balance, 1.5 mmol dodecane was added as internal standard. Unless otherwise stated, the catalyst was pretreated in a H₂:He gas flow (2:18 ml min⁻¹) at room temperature for an hour prior to use. The reaction flask was purged with helium followed by hydrogen before placing a hydrogen filled balloon over one of the necks. The other neck was closed off with a rubber septum. Under these conditions, the hydrogen pressure is very close to atmospheric throughout the reaction. Reactions were also carried out in a Berghof HR100 autoclave at 1 bar H₂ gauge (pressure maintained by

periodic topping up) and 30 °C. The reaction mixture consisting of 3 mmol (0.282 g) in 50 ml of cyclohexane as solvent was placed in a Teflon liner and an amount of catalyst corresponding to Rh: phenol mole ratio 1:100 was added. The system was purged with helium and heated. Once the temperature was stable, hydrogen gas was introduced to 1 bar gauge and the reaction was started. Aliquots were removed at regular time intervals and analyzed using an Agilent HP 6890 gas chromatograph (GC) equipped with a HP-5 column (30 m × 0.32 mm × 0.25 μm film) and a flame ionization detector. The GC program was as follows: initial temperature 60 °C, constant pressure, dwell time 8 min, ramp at 20 °C/min to 200 °C and hold for 3 min. The conversion and cyclohexanone selectivity were calculated based on the GC peak areas using experimentally determined calibration factors:

$$\text{Conversion (\%)} = \frac{C_{\text{cyclohexanone}} + C_{\text{cyclohexanol}}}{C_{\text{cyclohexanone}} + C_{\text{cyclohexanol}} + C_{\text{phenol}}}$$

$$\text{Cyclohexanone selectivity (\%)} = \frac{C_{\text{cyclohexanone}}}{C_{\text{cyclohexanone}} + C_{\text{cyclohexanol}}}$$

3. Results and discussion

3.1. Supported Rh catalysts

3.1.1. Textural properties

The x-ray diffractograms of the Rh/SiO₂ catalysts after calcination at 400 °C show only the broad peaks of amorphous SiO₂ (Fig. S1). No peaks of rhodium or rhodium oxide could be seen, even for the highest loading of 15 wt% Rh, suggesting that the Rh particle size is <5 nm. This is supported by TEM results where the average Rh particle size was between 1.59 and 3.66 nm for samples with 0.5–15 wt% Rh (Figs. 1 and S2). For each loading, the particles are narrowly distributed about the mean size with a standard deviation of 0.17–0.51 nm.

The nitrogen-sorption isotherms of all samples exhibit type IV isotherms with hysteresis at P/P⁰ ~ 0.7–0.9, indicating the presence of mesopores (Fig. 2). The SiO₂ support has a wide spread of pores from 5 to 23 nm with a mean pore size 17.8 nm. After impregnating with Rh, there was a shift to smaller pore sizes

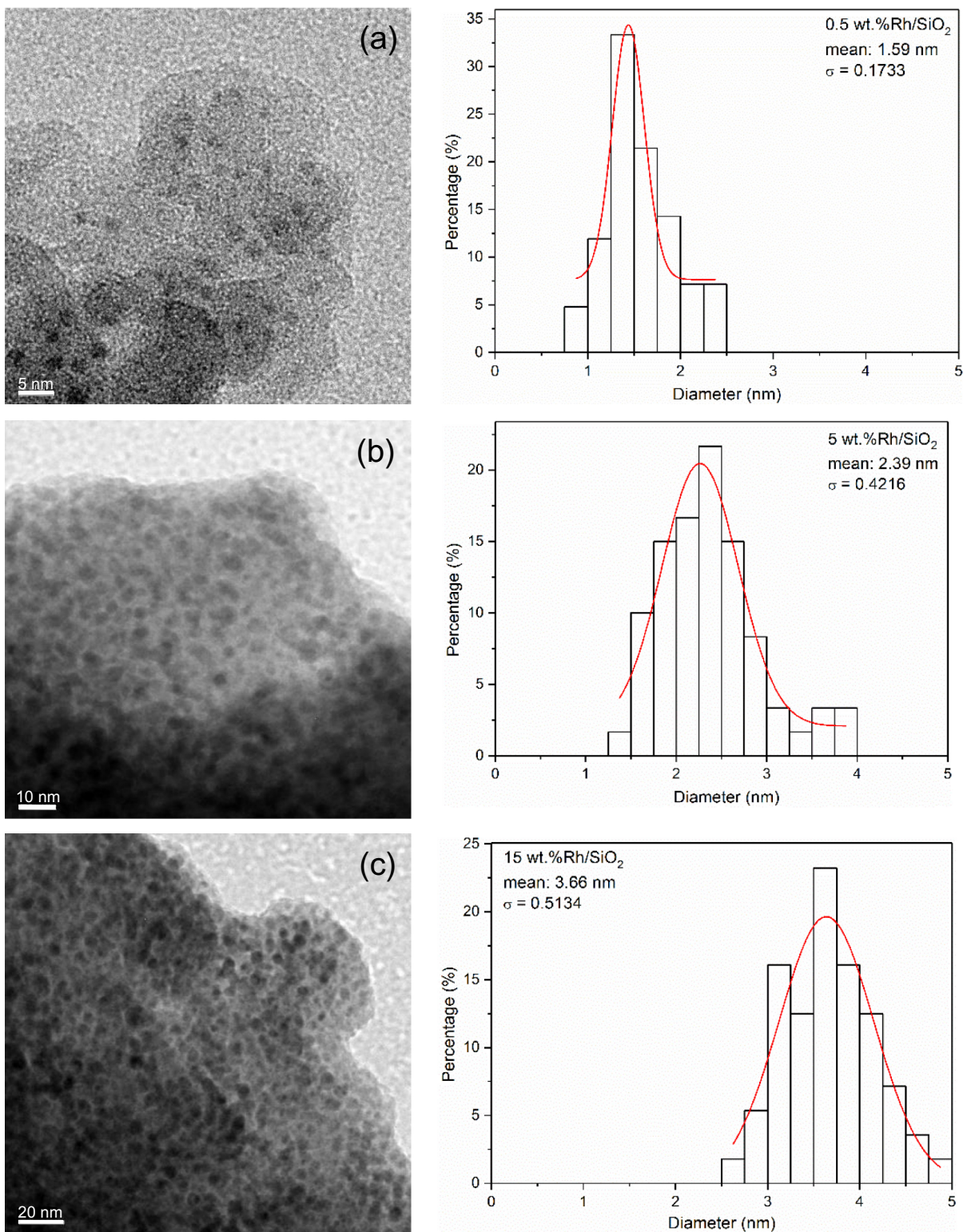


Fig. 1. TEM images and particle size distribution for (a) 0.5 (b) 5 and (c) 15 wt% Rh/SiO₂.

<18 nm. Irrespective of the Rh loading, the pore size distribution was rather similar with the mean at ~11.5 nm. Interestingly, SiO₂-H₂O, a sample prepared by the same wet impregnation procedure but using deionized water without any Rh, also suffered a similar decrease in pore size as well as pore volume. This shows that SiO₂ underwent textural changes with collapse of the larger pores as a result of the aqueous treatment. Despite this, the SiO₂

support has a high surface area in excess of 400 m² g⁻¹ even after calcination at 400 °C for 4 h (Table 2). With increase of Rh loading from 0 to 15 wt%, the surface area decreased from 406 to 324 m²/g and the pore volume dropped from 2.3 to 1.0 cm³ g⁻¹. The similarity of the pore size distribution curves suggests that the metal is uniformly distributed within the pore walls and no pore blockage occurred.

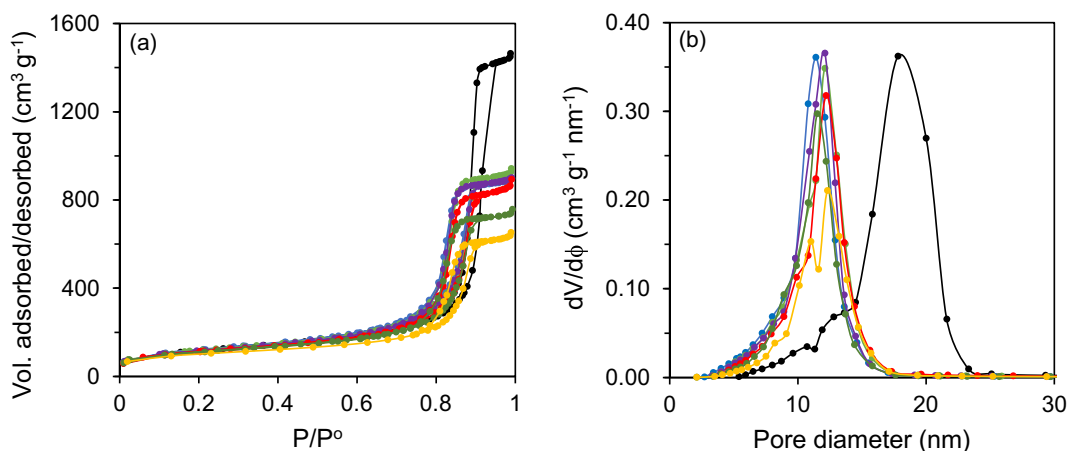


Fig. 2. (a) Nitrogen sorption isotherms and (b) pore size distribution of (●) SiO₂ (●) SiO₂-H₂O and Rh/SiO₂ catalysts with (●) 0.5 (●) 2 (●) 5 (●) 10 and (●) 15 wt% Rh.

Table 2
Textural properties of Rh/SiO₂ catalysts.

Rh loading (wt%)	Surface area (m ² g ⁻¹)	Pore volume (cm ³ g ⁻¹)	Mean Rh size (nm)
SiO ₂	406	2.3	–
SiO ₂ -H ₂ O	404	1.4	–
0.5	405	1.5	1.59
2	397	1.4	1.83
5	376	1.4	2.39
10	367	1.2	3.25
15	324	1.0	3.66

3.1.2. Catalytic activity

3.1.2.1. Effect of support. The hydrogenation of phenol was carried out at 25 °C and 1 atm H₂ pressure in cyclohexane. A preliminary study carried out using different solvents showed that the highest yield of cyclohexanone was obtained with cyclohexane (Table S1). Moreover, it has a low boiling point 80.74 °C, which facilitates separation from the higher boiling products.

Samples containing 5 wt% Rh supported on various supports were tested. Good activity was obtained for the SiO₂-supported sample. Even without any pre-reduction of the catalyst, 100% conversion and 82% selectivity to cyclohexanone was obtained

after 9 h under these mild conditions (Table 3, entry 1). Pretreating the catalyst to a 10% oxygen in helium flow mixture at 300 °C for 1 h did not affect the activity and selectivity, which were essentially similar to that of the untreated catalyst (Table 3, entry 2). In contrast, after pre-reduction at 300 °C for 1 h under a gas flow of 10% H₂ in helium, full conversion was reached in a much shorter time of 3.5 h (Table 3, entry 3). However, the selectivity to cyclohexanone was reduced to 68% as further hydrogenation to cyclohexanol occurred. With a gentler reduction at room temperature instead of 300 °C, 100% phenol conversion was obtained in 5 h and the cyclohexanone selectivity was 80% (Table 3, entry 4). Conducting the reactions in an autoclave gave very similar results. Due to the higher pressure of 1 bar H₂ pressure and 30 °C, full phenol conversion could be achieved in a shorter time of 3–4 h (Table 3, entries 5 and 6).

TiO₂-supported Rh samples also do not need any pre-reduction. Over an unreduced 5 wt% Rh/TiO₂, 70% of the phenol was converted to cyclohexanone after 10 h (Table 3, entry 7). The cyclohexanone selectivity at 80% was similar to that for the SiO₂-supported sample. In contrast, the as-formed La₂O₃-, MgO-, ZrO₂-supported Rh catalysts were inactive and had to be reduced (Table 3, entries 9–14). After reduction at 300 °C for 1 h, phenol was fully converted after 3.5 h over Rh/ZrO₂ but required a longer time of 24 h for

Table 3
Selective hydrogenation of phenol over 5 wt% Rh and Pd catalysts.

Entry	Catalyst	Pretreatment	Reaction Conditions ^[a]	Time (h)	Conv. (%)	Sel. C=O (%)
1	Rh/SiO ₂	None	Balloon	9	100	82.6
2	Rh/SiO ₂	Oxidized ^[b]	Balloon	9	100	82.8
3	Rh/SiO ₂	Reduced ^[c]	Balloon	3.5	100	68.1
4	Rh/SiO ₂	Reduced ^[d]	Balloon	5	100	80.5
5	Rh/SiO ₂	Oxidized ^[b]	Autoclave	4	100	80.6
6	Rh/SiO ₂	Reduced ^[c]	Autoclave	3	100	53.1
7	Rh/TiO ₂	None	Balloon	10	70	80.5
8	Rh/TiO ₂	Reduced ^[c]	Balloon	3	100	72.1
9	Rh/La ₂ O ₃	None	Balloon	24	0	0
10	Rh/La ₂ O ₃	Reduced ^[c]	Balloon	24	100	74.3
11	Rh/MgO	None	Balloon	24	0	0
12	Rh/MgO	Reduced ^[c]	Balloon	7	100	73.5
13	Rh/ZrO ₂	None	Balloon	24	0	0
14	Rh/ZrO ₂	Reduced ^[c]	Balloon	3.5	100	78.2
15	Pd/C	None	Balloon	48	11.1	100
16	Pd/C	Reduced ^[c]	Balloon	48	84.2	82.4

^[a] Reaction conditions: balloon – phenol (1.5 mmol), cyclohexane (25 ml), catalyst (0.03 g), H₂ in balloon, 25 °C; autoclave – phenol (3 mmol), cyclohexane (50 ml), catalyst (0.06 g), 1 bar gauge H₂ pressure in autoclave, 30 °C.

^[b] Catalyst pre-oxidized at 300 °C for 1 h in O₂/He gas flow (2:18 ml min⁻¹).

^[c] Catalyst pre-reduced at 300 °C.

^[d] Room temperature for 1 h in H₂/He gas flow (2:18 ml min⁻¹).

Rh/La₂O₃. Despite the different activity of the catalysts, the selectivity to cyclohexanone was relatively similar, ~73–78%. A commercial 5 wt% Pd/C catalyst was tested for comparison (Table 3, entries 15 and 16). Under the experimental conditions, 25 °C and 1 atm hydrogen, its activity was low. The reduced catalyst required 48 h to reach 84% conversion with 82% selectivity to cyclohexanone.

The kinetics of the reaction were monitored using the 5 wt% Rh/SiO₂. Without any pre-reduction of the catalyst, no phenol was converted within the first 2 h when the reaction was carried out with H₂ contained in a balloon at atmospheric pressure (Fig. 3a). After this induction time, phenol was converted to cyclohexanone and cyclohexanol. No other products were formed (Fig. S3). The selectivity to cyclohexanone was ~82% and remained constant until all the phenol was converted. Extending the reaction beyond this time led to the rapid hydrogenation of cyclohexanone to cyclohexanol. The mass balance closed to within 2% (Fig. S4). In contrast to the unreduced catalyst, after pretreatment in 10% H₂/He flow for an hour at room temperature, the reaction commenced from the start (Fig. 3b). Similarly, no induction period was observed when the reaction was carried out in an autoclave (Fig. S5). This can be attributed to a more rapid reduction of the catalyst under 1 bar gauge H₂ pressure at 30 °C. The constant selectivity of about 18% cyclohexanol immediately from the start of the reaction shows that there are sites that catalyse the complete hydrogenation of phenol to cyclohexanol and those that catalyse only partial hydrogenation to cyclohexanone. Only after all the phenol has been converted does hydrogenation of the formed

cyclohexanone occur. Obviously, the latter sites can hydrogenate phenol as well as cyclohexanone. Therefore, the adsorption of phenol at these sites must be much stronger than that of cyclohexanone so that even at low phenol concentration, little cyclohexanone was hydrogenated.

The results show that the metallic state of rhodium is necessary for reaction. For TiO₂- and SiO₂-supported samples, this can be effected under very mild conditions either *in-situ* or *ex-situ*, at 1 atm H₂ pressure and room temperature. In contrast, Rh supported on La₂O₃, MgO or ZrO₂ required a high temperature (300 °C) reduction. Hence, SiO₂ was chosen as the support for further studies due to its high activity for the selective hydrogenation of phenol at 25 °C and atmospheric H₂ pressure and its ease of handling.

3.1.2.2. Effect of metal loading. The reactions were conducted in an autoclave using 1 bar gauge H₂ at 30 °C due to the faster kinetics. No reaction was observed over the SiO₂ support (Table 4). However, a low Rh loading of 0.5 wt% resulted in a highly active catalyst with all phenol being converted after only 3.5 h (Fig. 4a). The initial selectivity to cyclohexanone and cyclohexanol was ~75% and 25%, respectively. This ratio remained fairly constant until all the phenol was consumed whereupon rapid hydrogenation of cyclohexanone to cyclohexanol occurred. Similar kinetic profiles were observed for 2–10 wt% Rh/SiO₂ although full phenol conversion required longer times of 5 to 8 h (Fig. S5). The initial cyclohexanone selectivity increased to 82–85% with higher Rh loading. At full conversion, 5 wt% Rh/SiO₂ has the highest selectivity of 80.5%. In contrast, the

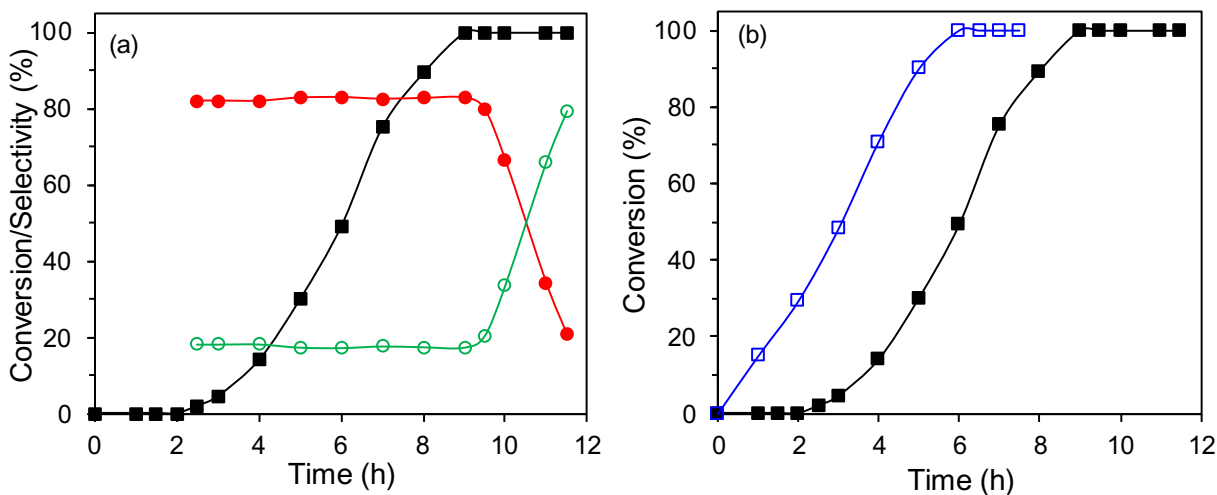


Fig. 3. (a) Time profile for 5 wt% Rh/SiO₂ (■) conversion and selectivity to (●) cyclohexanone and (○) cyclohexanol. (b) Conversion for (■) untreated catalyst and (□) after H₂ pretreatment at room temperature for 1 h. Reaction conditions: phenol (1.5 mmol), cyclohexane (25 ml), catalyst (0.03 g), H₂ in balloon, 25 °C. Standard deviation from 3 catalytic runs: conversion ± 1.6%, selectivity ± 0.5%.

Table 4
Selective hydrogenation of phenol over Rh/SiO₂ catalysts.^[a]

Entry	Rh (wt%)	Time (h)	Conv. (%)	Sel. (%)	Conv. ^[b] (%)	Sel. ^[b] (%)	TOF ^[b] (h ⁻¹)	N _s /N _r	D ^[c] (%)
1	0	24	0	0	0	–	0	–	–
2	0.5	3.5	100	69.1	12.5	75.6	41	0.62	68.3
3	2	5	100	73.2	10.3	81.4	37	0.56	55.7
4	5	5	100	80.5	8.5	83.8	38	0.46	45.6
5	10	7	100	65.3	6.3	84.8	36	0.36	34.6
6	15	15	100	35.1	3.1	86.2	26	0.32	31.5

^[a] Reaction conditions: phenol (3 mmol), cyclohexane (50 ml), catalyst (0.06 g), 1 bar H₂ pressure in autoclave at 30 °C.

^[b] Conversion and selectivity to cyclohexanone after 0.5 h. Standard deviation from 3 catalytic runs: conversion ± 1.6%, selectivity ± 0.5%.

^[c] Rh dispersion from CO chemisorption.

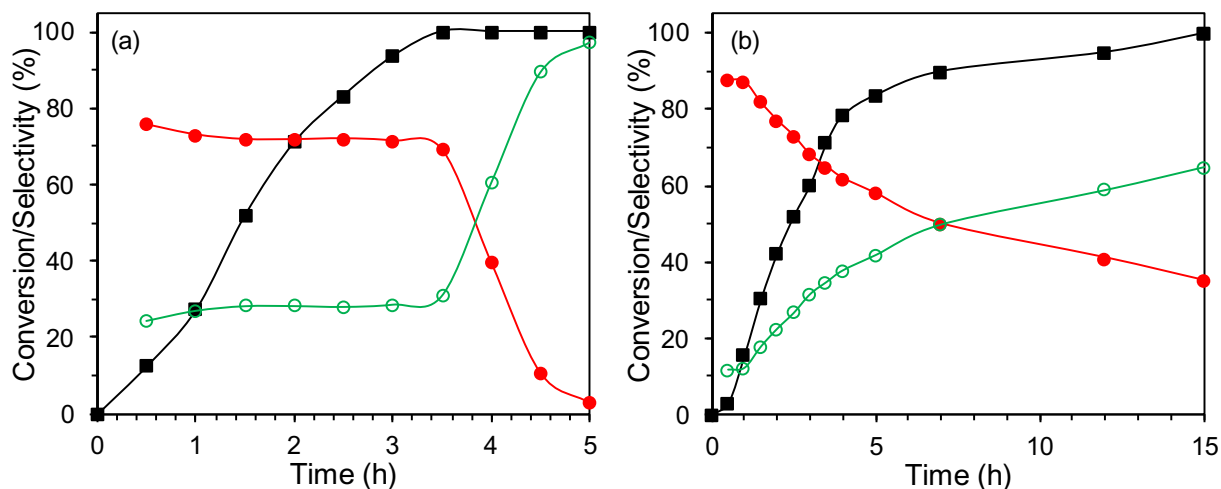


Fig. 4. (a) Time profile of (a) 0.5 and (b) 15 wt% Rh/SiO₂ (■) conversion and selectivity to (●) cyclohexanone and (○) cyclohexanol. Reaction conditions: phenol (3 mmol), cyclohexane (50 ml), phenol/Rh 100:1 (mole ratio), 1 bar H₂ pressure in autoclave at 30 °C. Standard deviation from 3 catalytic runs: conversion ± 1.6%, selectivity ± 0.5%.

15 wt% Rh/SiO₂ sample displayed different reaction kinetics (Fig. 4b). Although the initial cyclohexanone selectivity was high, 86%, it began to decrease with increasing conversion even when phenol was still present. Finally, at 100% phenol conversion, the selectivity to cyclohexanone was reduced to only 35%.

The results clearly show that the metal loading affects the activity for phenol hydrogenation and selectivity to cyclohexanone. As observed by TEM (Fig. 1), the increase in metal loading leads to larger particles. From CO chemisorption measurements, metal dispersion fell from 68.3 to 31.5% for 0.5 to 15 wt% Rh (Table 4). The number of atoms at the surface, N_s , and the total atoms in a particle, N_T , can also be estimated from the atomic size and crystal structure of Rh [43–45]. The ratio N_s/N_T decreased from 0.62 to 0.32 as the Rh loading increased from 0.5 to 15 wt% (Table 4). These values are in good agreement with those obtained by CO chemisorption.

Infrared spectroscopy of adsorbed CO was used to probe the site distribution of the surface Rh atoms (Fig. 5). The IR spectrum of 0.5 wt% Rh/SiO₂ show bands at ~2098 and ~2038 cm⁻¹, which are assigned to the symmetric and asymmetric modes of geminal Rh(CO)₂, respectively [46–48]. The presence of these bands is reflective of coordinatively unsaturated Rh centers or dispersed clusters [22,49]. With higher Rh loading, bands at ~2065 and

~1960 cm⁻¹ appeared which are assigned to linearly-bonded Rh-CO and bridged CO-Rh of 3:2 stoichiometry [42]. Furthermore, for 15 wt% Rh/SiO₂, the small band at ~1840 cm⁻¹ is characteristic of bridged-bonded Rh(CO)₂ [42]. The linear- and bridged-bonded CO are ascribed to crystalline Rh found on larger particles [49]. These results show changes in type of sites with particle growth. As steps and kink sites are more reactive than terrace sites, it is not surprising that the initial turnover frequency (TOF) per surface atom was highest at 41 h⁻¹ for 0.5 wt% Rh. For 2–10 wt% Rh, the TOF was rather constant at ~37 h⁻¹ and decreased to 26 h⁻¹ for 15 wt% Rh. The high TOF for 0.5 wt% Rh/SiO₂ is due to a higher rate of cyclohexanol formation as its TOF for cyclohexanone formation was similar to catalysts with higher Rh loading (Fig. S6).

Using density functional theory (DFT), Honkela et al found that the adsorption and dissociation of phenol on flat Rh(1 1 1) surface was preferred over that of stepped Rh(2 1 1) due to repulsion of the hydroxyl group from the step edges [50]. Li et al. also investigated the role of phenol dissociation in the selective hydrogenation on Pt(1 1 1) and Pd(1 1 1) using DFT slab calculations [51]. The calculated energetics and activation barriers indicate that hydrogenation of phenoxy leads to cyclohexanone while direct hydrogenation of adsorbed phenol results in cyclohexanol. Therefore, to gain some insights into the site differentiation on selectivity, DFT calculations were performed with the Vienna ab initio simulation package (VASP) [52,53]. The projector-augmented wave method with PBE exchange-correlation functional was used and the cut-off energy was set as 400 eV [54]. The DFT-D3 method with Becke-Jonson damping was adopted to include van der Waals interactions [55,56]. All structures were relaxed using a conjugate-gradient algorithm until the residual force was smaller than 0.02 eV/Å. The climbing-image nudged elastic band method was used for transition state search and activation energy calculation [57]. Rh(1 1 1) was chosen as representative of a big particle with flat plane. The Rh(1 1 1) surface modelled by a 3-layer slab model with the bottom layer fixed at their bulk positions. A 6-atom Rh cluster supported on silica was further studied to evaluate the size effect on the dissociation of the hydroxyl in phenol. The cleavage barrier for O–H bond was found to be 0.557 eV for phenol adsorbed on Rh(1 1 1) surface as compared to 1.354 for the 6-atom cluster (Fig. S7). Hence, the dissociation of phenol to phenoxy is easier on flat surfaces than on small clusters.

Based on our results, we propose the following. Firstly, at least two different sites are involved for phenol hydrogenation, one

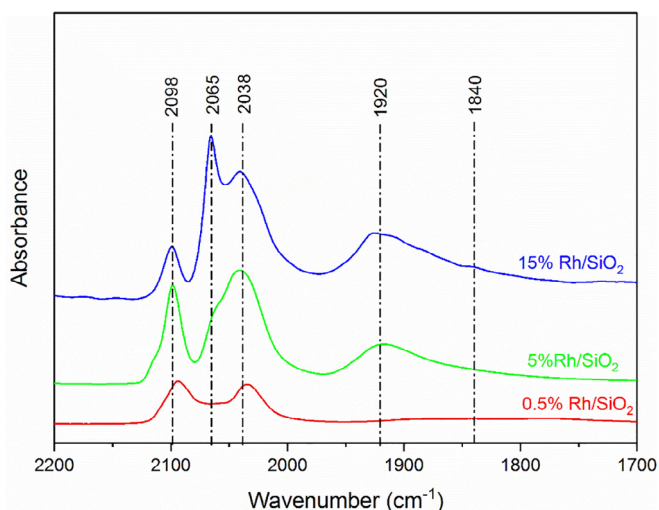


Fig. 5. Infrared spectra of CO chemisorbed on Rh/SiO₂ at room temperature.

catalyzing the direct hydrogenation to cyclohexanol (site 1) and the other (site 2) via cyclohexanone (Fig. 6a). As direct hydrogenation to cyclohexanol was most prominent for the highly dispersed 0.5 wt% Rh/SiO₂, it suggests that site (1) comprises Rh atoms at corners and edges. Being coordinatively unsaturated, they exhibit excellent activity for reactions including hydrogen dissociation. Consequently, there are abundant H atoms to hydrogenate phenol directly to cyclohexanol. The fraction of such sites decreases with bigger clusters, and is paralleled by a decrease in the initial cyclohexanol selectivity with Rh loading. Site (2) comprises atoms on planes and terraces that predominate in larger particles. As shown by computational studies, these are preferred sites for phenol adsorption and dissociation [50].

Secondly, the observation that hydrogenation of cyclohexanone occurs only after all the phenol has been consumed shows that phenol adsorbs more strongly than cyclohexanone. More importantly, it also suggests that the sites are independent of each other, i.e., site (1) does not catalyze the hydrogenation of cyclohexanone formed at site (2), otherwise increasingly more cyclohexanol would be formed with time. Only the 15 wt% Rh/SiO₂, which had the largest particle size and hence adequate density of planar sites, was able to catalyze both phenol and cyclohexanone hydrogenation simultaneously so that at full conversion, the cyclohexanone selectivity was the lowest. The other lower Rh-containing samples were able to give higher cyclohexanone yields as the cyclohexanone selectivity was maintained until all the phenol was converted.

The independence of the two hydrogenation sites and striking feature that cyclohexanone is only reduced in the absence of phenol offer a chance to improve the selectivity to cyclohexanol. We envisage that if site (1), responsible for direct hydrogenation of phenol to cyclohexanol, could be deactivated or removed, the formation of cyclohexanol would be minimized. In order to achieve this, amine, chloro- and thiol-containing molecules were grafted using the chemical reaction between hydroxyl groups at the catalyst surface and substituted trimethoxysilanes. Those molecules positioned adjacent to the sides of the metal particle can hinder

access of the reactant molecule to the neighbouring low coordination sites (Fig. 6b). In a previous study, the group of Dyson reported that the chemoselectivity in the hydrogenation of acetophenone to cyclohexylacetone could be modified by the addition of phosphine ligands to PVP-stabilized Rh nanoparticles [58]. It was postulated that specific sites at the surface of the nanoparticles became blocked although the nature of these sites were not investigated.

3.2. Grafting modification on Rh/SiO₂

3.2.1. Catalytic activity

Trialkoxysilanes containing NH₂, Cl, S and O functional moieties (Table 1) were grafted onto the 5 wt% Rh/SiO₂ catalyst. The grafted catalysts showed lower hydrogenation activity than the unmodified 5 wt% Rh/SiO₂ which can be attributed to partial coverage of the Rh surfaces by the organic molecules (Table 5). Samples grafted with NH₂, Cl and O functional moieties showed lower or comparable cyclohexanone selectivity to that for 5 wt% Rh/SiO₂. In contrast, the cyclohexanone selectivity was increased from 82 to 87% for the sample grafted with (3-mercaptopropyl)trimethoxy silane. However, its conversion was only 47% even after 24 h. To try

Table 5
Selective hydrogenation of phenol to cyclohexanone over grafted 5 wt% Rh/SiO₂.

Entry	Catalyst	Time (h)	Conv. (%)	Sel. (%)
1	5 wt%Rh/SiO ₂	9	100	82
2	Glycidyl-5 wt%Rh/SiO ₂	25	100	82
3	Aniline-5 wt%Rh/SiO ₂	10	100	80
4	Chloro-5 wt%Rh/SiO ₂	24	100	60
5	Thiol-5 wt%Rh/SiO ₂	24	47	89
6 ^[a]	Thiol-5 wt%Rh/SiO ₂	10	100	93
7	Amine-1-5 wt%Rh/SiO ₂	8.5	100	86
8	Amine-2-5 wt%Rh/SiO ₂	24	42	72
9	Amine-3-5 wt%Rh/SiO ₂	24	15	84

Reaction conditions: phenol (1.5 mmol), cyclohexane (25 ml), catalyst (0.03 g), H₂ (1 atm, balloon), 25 °C.

^[a] Pretreated in O₂/He gas flow (2:18 ml/min) at 200 °C for 1 h.

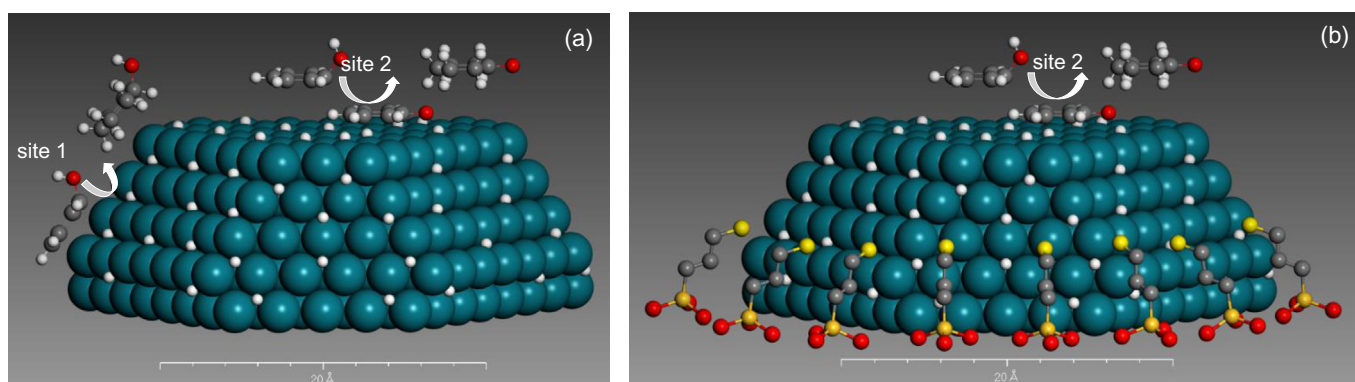
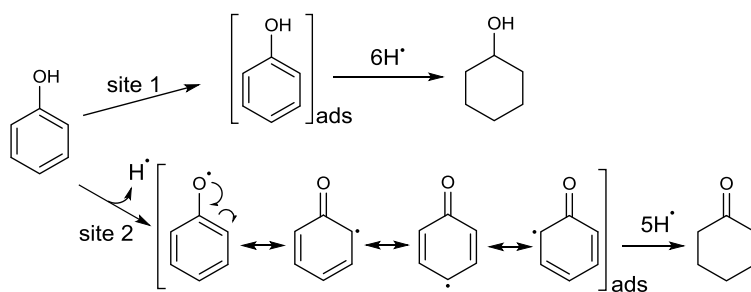


Fig. 6. (a) Schematic diagram showing the coordinatively unsaturated (*cus*) site (1) for direct hydrogenation of phenol to cyclohexanol and terrace site (2) for partial hydrogenation of phenol to cyclohexanone (b) blocking of *cus* sites at sides of particles by grafted (3-mercaptopropyl)silane groups.

and improve its activity, the Thiol-grafted catalyst was preheated in a 10% O₂/He gas mixture at 200 °C for 1 h so as to pyrolyse some of the thiol groups presumably covering the Rh metal. This pre-treatment proved to be very effective as full conversion could be obtained after 10 h (Fig. 7a). The results for three series of Thiol-grafted catalyst are consistent and showed that the initial selectivity to cyclohexanone was ~98% and decreased slightly to 91–93% for conversions higher than 30% (Fig. 7b). The selectivity remained fairly constant even as the conversion increased to 100%.

To gain some insights, both the Rh/SiO₂ and Thiol-grafted catalysts were tested for hydrogenation of cyclohexanone and cyclohex-2-enone. The Rh/SiO₂ catalyst showed good activity for

the conversion of cyclohexanone to cyclohexanol, with 100% conversion after 6 h at 1 atm H₂ pressure. (Table 6, entry 1). In comparison, over the Thiol-grafted catalyst, the conversion was only 28% after 12 h despite the use of 2 bar gauge H₂ pressure, showing that grafting with the thiol moiety significantly blocked the active sites for C=O hydrogenation (Table 6, entry 2). Similarly, the hydrogenation of cyclohex-2-enone to cyclohexanone was also slower for the Thiol-grafted catalyst as compared to Rh/SiO₂ (Table 6, entries 3 & 4).

Substituted phenols (Table 6, entries 5–18) were also selectively hydrogenated to the corresponding carbonyl products with a higher selectivity over the grafted catalyst than the ungrafted

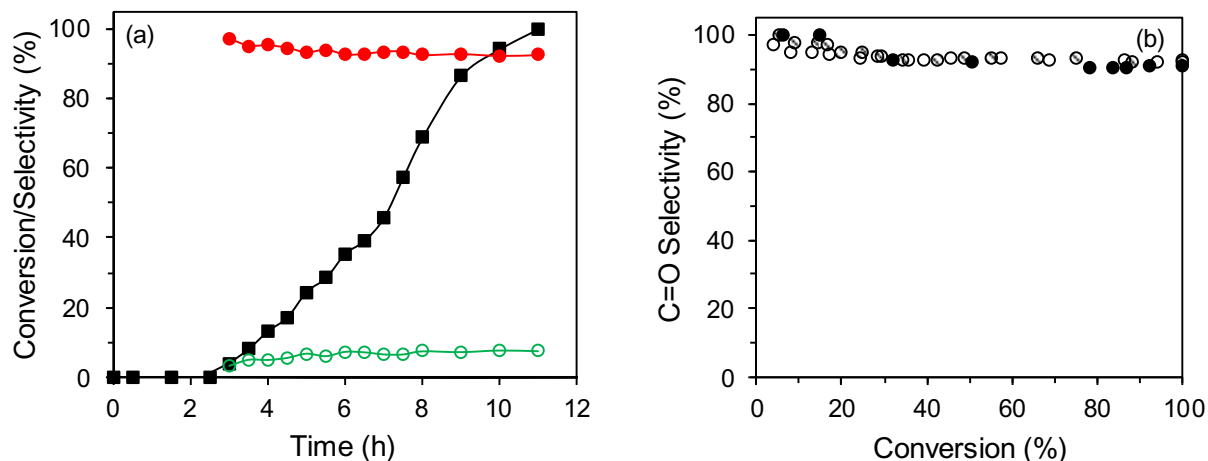


Fig. 7. (a) Time profile of Thiol-5 wt% Rh/SiO₂ after pretreatment in a 10% O₂/He gas mixture at 200 °C for 1 h (■) conversion and selectivity to (●) cyclohexanone and (○) cyclohexanol (b) cyclohexanone selectivity versus conversion for three series of Thiol-5 wt% Rh/SiO₂. Reaction conditions: phenol (1.5 mmol), cyclohexane (25 ml), catalyst (0.03 g), 1 atm H₂ in balloon at 25 °C. Standard deviation from 3 catalytic runs: conversion ± 1.8%, selectivity ± 0.4%.

Table 6
Selective hydrogenation with 5 wt% Rh/SiO₂ and Thiol-5 wt% Rh/SiO₂.

Entry	Catalyst	Rxn	Substrate	Time (h)	Product	Conv. (%)	Sel. (%)
1	Rh	Balloon		6		>99	>99
2	Thiol	Autoclave		12		28	>99
3	Rh	Balloon		3.5		>99	96
4	Thiol	Autoclave		4.5		>99	>99
5	Rh	Balloon		9.5		>99	77
6	Thiol	Balloon		28		>99	>99
7	Thiol	Autoclave		6		>99	93
8	Rh	Balloon		12		>99	75
9	Thiol	Balloon		30		65	92
10	Thiol	Autoclave		6		>99	85
11	Rh	Balloon		20		>99	73
12	Thiol	Balloon		24		9	89
13	Thiol	Autoclave		6		57	81
14	Rh	Balloon		10		>99	80
15	Thiol	Balloon		24		57	>99
16	Thiol	Autoclave		6		83	94
17	Rh	Balloon		28		>99	76
18	Thiol	Balloon		30		10	>99
19	Thiol	Autoclave		6		48	83
20	Rh	Balloon		15		>99	41
21	Thiol	Balloon		30		5	89
22	Thiol	Autoclave		6		39	73

Reaction conditions: phenol (1.5 mmol), cyclohexane (25 ml), catalyst (0.03 g), H₂ in balloon at 25 °C or in autoclave at 2 bar gauge H₂ and 30 °C.

Rh/SiO₂. For example, >99% selectivity to the ketone was observed in the hydrogenation of *p*-cresol, 4-*tert*-butylphenol, and 4-methoxyphenol. Hence, grafting of Rh/SiO₂ with (3-mercaptopropyl)trimethoxysilane formed a selective catalyst for hydrogenation of phenol to cyclohexanone under mild conditions of room temperature and one atm H₂ pressure.

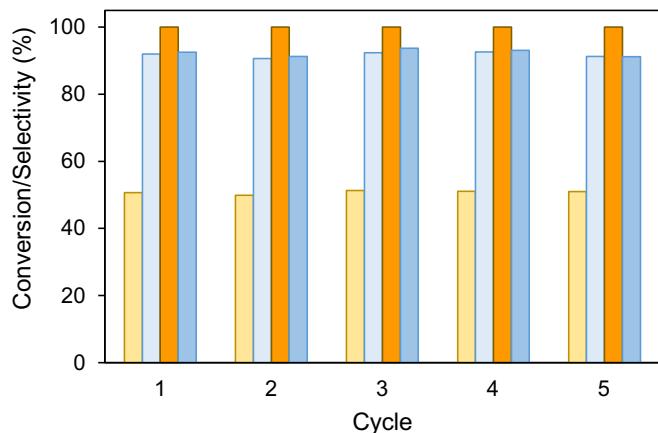


Fig. 8. Conversion and selectivity at 5 h (■) and 11 h (■) reaction over recycled Thiol-5 wt% Rh/SiO₂.

After reaction, the used Thiol-5 wt% Rh/SiO₂ catalyst was recovered by centrifugation, washed with ethanol and dried at room temperature. When reused for up to five cycles, it was able to maintain its activity and high selectivity for cyclohexanone (Fig. 8). No Rh could be detected in the reactant mixture by ICP-AES, confirming the stability of the catalyst. The surface area and pore volume of the recycled catalyst were slightly decreased by ~10% compared to the fresh one (Fig. S8). The Rh dispersion of recycled catalyst was not significantly affected with reuse, ~41%.

3.2.2. Nature of Thiol-5 wt% Rh/SiO₂

Thermogravimetric analysis (TGA) was used to determine the amount of organic component in the Thiol-grafted Rh/SiO₂ sample. For comparison, the SiO₂ support was also grafted with (3-mercaptopropyl)trimethoxysilane. The weight loss below 450 °C was ~4.77% for both samples (Fig. S9). Use of TGA-MS showed that the weight loss can be attributed to desorption of water and pyrolysis of the (3-mercaptopropyl)trimethoxysilane moiety (Fig. S10). After some of the thiol moiety was pyrolyzed during pretreatment in a flow of 10% O₂/He for 1 h at 200 °C, smaller weight losses of 1.86% and 1.3% were determined for the catalyst and support, respectively. From the results, ~0.20 mmol/g of (3-mercaptopropyl)trimethoxysilane remained on the catalyst. The presence of (3-mercaptopropyl)trimethoxysilane was confirmed by IR measurements (Fig. S11). Absorption bands at ~2930, 2868 and 2549 cm⁻¹ were observed. The first two can be assigned to the asymmetric and

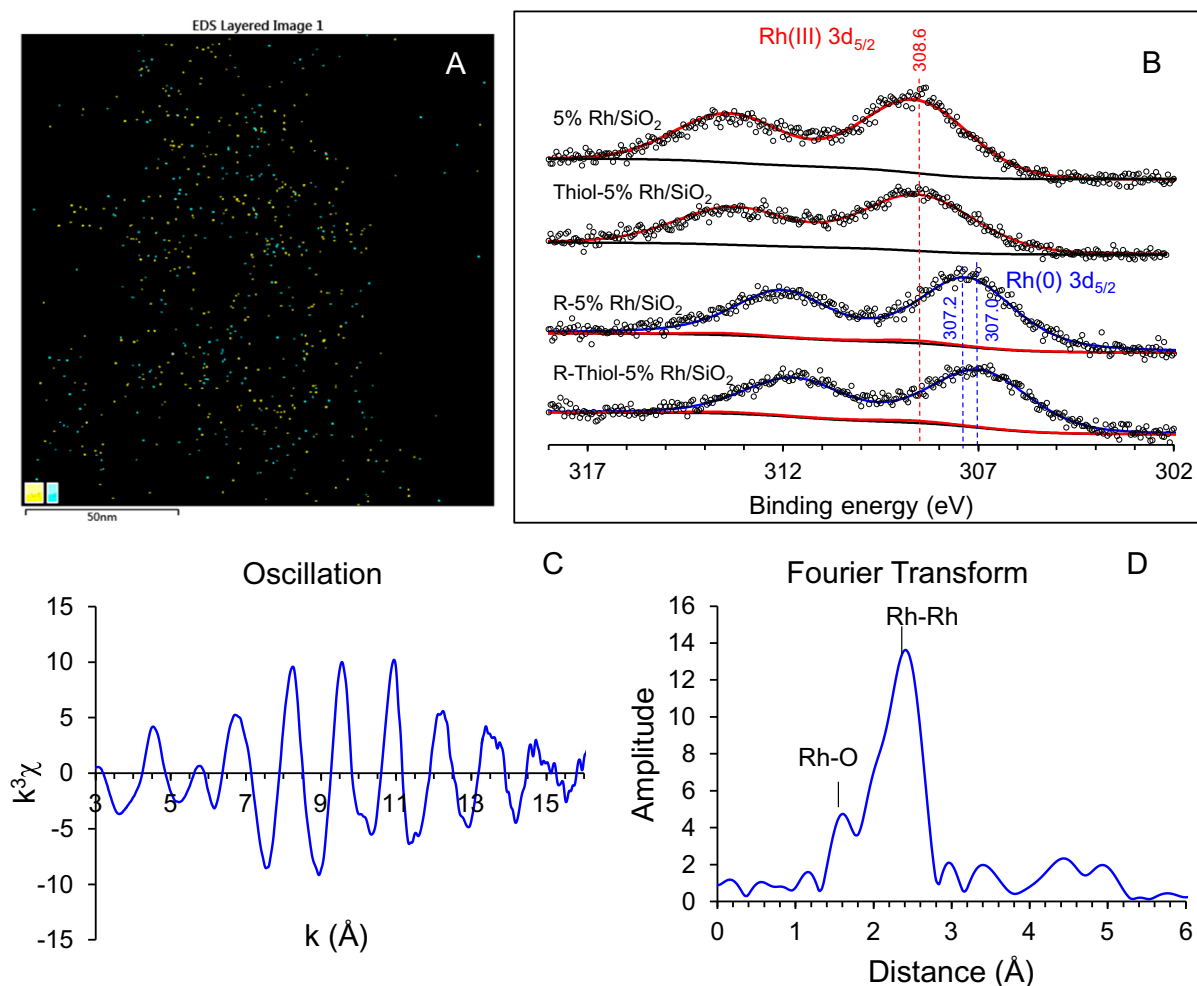


Fig. 9. (A) EDS for Rh and S in Thiol-5 wt% Rh/SiO₂ (B) XPS spectra of as-prepared 5 wt% Rh/SiO₂ and Thiol-5 wt% Rh/SiO₂ and after reduction in H₂/He flow at 25 °C; (C) experimental χ data with k^3 weighting and (D) Fourier transformed k^3 -weighted χ function for Thiol-5 wt% Rh/SiO₂.

symmetric CH₂ stretching of the propylic chain, respectively while the 2549 cm⁻¹ band is characteristic of the S-H stretching mode [59]. Compared to 5 wt% Rh/SiO₂, the IR spectrum of chemisorbed CO of the Thiol-grafted sample showed a slightly more pronounced band of the linearly-bonded CO at 2090 cm⁻¹ while the band due to bridge-bonded CO is shifted to lower wavenumbers (Fig. S12). The differences, although small, point to more planar sites being accessed by CO. EDS mapping showed that the sulfur is well dispersed in the proximity of rhodium (Fig. 9A and S13).

XPS measurements revealed that Rh³⁺ was the predominant surface species in 5 wt% Rh/SiO₂ and Thiol-5 wt% Rh/SiO₂ (Fig. 9B). However, after a mild treatment in H₂ at room temperature for 1 h, the Rh 3d_{5/2} binding energy was shifted to 307.2 and 307.0 eV for the Rh/SiO₂ and Thiol-Rh/SiO₂ samples, respectively. These values fall into the expected binding energy for Rh⁰ [60–63]. However, the binding energy was lower in grafted sample which suggests a higher electron density at the Rh atom. This could be due to electron donation from the neighbouring sulfur on the (3-mercaptopropyl) group. In order to check if any Rh-S bond could be discerned, EXAFS measurements were conducted on the Thiol-5 wt% Rh/SiO₂ sample that had been pretreated in H₂/He at room temperature. The EXAFS spectrum showed a rapid oscillation on the Rh K edge (Fig. 9C). In the Fourier transformed EXAFS function, two peaks can be observed (Fig. 9D). The peak at 2.4 Å can be assigned to the Rh-Rh bond length while that at 1.6 Å corresponds to the Rh-O bond distance [61]. The bulk of rhodium is in the metallic form, in agreement with the XPS results. Although no Rh-S bond could be discerned, the adsorption and further hydrogenation at the C=O end of cyclohexanone is less likely due to repulsion from the electron-rich Rh. Hence, both steric and electronic effects could be responsible for the improved cyclohexanone selectivity in the thiol-grafted catalyst.

4. Conclusion

Supported Rh catalysts were evaluated for the selective hydrogenation of phenol to cyclohexanone at room temperature and 1 atm H₂ pressure. SiO₂- and TiO₂-supported Rh could be easily reduced under reaction conditions or *ex-situ* under flowing hydrogen at room temperature, in contrast to the need for high temperature activation for La₂O₃, MgO and ZrO₂-supported samples. With increase of Rh loading from 0.5 to 15 wt% on SiO₂, nanoparticles of 1.59–3.66 nm were formed. The catalytic hydrogenation of phenol forms both cyclohexanol and cyclohexanone from the start of reaction. At constant phenol:Rh mole ratio of 100:1, the catalytic activity decreased whereas the initial selectivity to cyclohexanone increased with Rh particle size. It was proposed that coordinatively unsaturated sites such as kinks and steps catalyse the direct hydrogenation of phenol to the final product, cyclohexanol, whereas higher coordinated terrace sites catalyse the partial hydrogenation to cyclohexanone. DFT calculations indicated that dissociation of phenol was more facile on flat surfaces than small particles. Grafting a 5 wt% Rh/SiO₂ catalyst with (3-mercaptopropyl)trimethoxysilane improved the cyclohexanone selectivity from 82% to 93% at 100% conversion. This was attributed to a steric effect where access to the coordinatively unsaturated sites was blocked. Hence, an active, selective and recyclable rhodium-based catalyst has been developed for the selective hydrogenation of phenol to cyclohexanone under mild conditions.

Acknowledgements

This work was supported by the Academic Research Grant, R-143-000-667-114, National University of Singapore. The award of an NUS research scholarship for H. W. Zhang is gratefully acknowledged.

Appendix A. Supplementary material

Supplementary data associated with this article can be found, in the online version, at <https://doi.org/10.1016/j.jcat.2018.06.002>.

References

- [1] S. Van de Vyver, Y. Román-Leshkov, Catal. Sci. Technol. 3 (2013) 1465–1479.
- [2] Cyclohexanol and Cyclohexanone, Chemical Economics Handbook IHS Markit, 2017.
- [3] M.T. Musser, Cyclohexanol and cyclohexanone, Ullmann's Encyclopedia Indus. Chem. (2011), https://doi.org/10.1002/14356007.a08_217.pub2.
- [4] H. Jiang, Z. Qu, Y. Li, J. Huang, R. Chen, W. Xing, Chem. Eng. J. 284 (2016) 724–732.
- [5] E. Simón, J.M. Rosas, A. Santos, A. Romero, Catal. Today 187 (2012) 150–158.
- [6] Y. Wang, J. Yao, H. Li, D. Su, M. Antonietti, J. Am. Chem. Soc. 133 (2011) 2362–2365.
- [7] H. Liu, T. Jiang, B. Han, S. Liang, Y. Zhou, Science 326 (2009) 1250–1252.
- [8] L.M. Sikhwithlu, N.J. Coville, D. Naresh, K.V. Chary, V. Vishwanathan, Appl. Catal., A 324 (2007) 52–61.
- [9] J. Morales, R. Hutcheson, C. Noradoun, I.F. Cheng, Ind. Eng. Chem. Res. 41 (2002) 3071–3074.
- [10] S. Srinivas, P.K. Rao, J. Catal. 179 (1998) 1–17.
- [11] P. Claus, H. Berndt, C. Mohr, J. Radnik, E.-J. Shin, M.A. Keane, J. Catal. 192 (2000) 88–97.
- [12] M. Zhao, J. Shi, Z. Hou, Chin. J. Catal. 37 (2016) 234–239.
- [13] L. Cheng, Q. Dai, H. Li, X. Wang, Catal. Commun. 57 (2014) 23–28.
- [14] D. Zhang, Y. Guan, E.J.M. Hensen, L. Chen, Y. Wang, Catal. Commun. 41 (2013) 47–51.
- [15] Y. Pérez, M. Fajardo, A. Corma, Catal. Commun. 12 (2011) 1071–1074.
- [16] M. Chatterjee, H. Kawanami, M. Sato, A. Chatterjee, T. Yokoyama, T. Suzuki, Adv. Synth. Catal. 351 (2009) 1912–1924.
- [17] P. Makowski, R.D. Cakan, M. Antonietti, F. Goettmann, M.-M. Titirici, Chem. Commun. (2008) 999–1001.
- [18] J. Matos, A. Corma, Appl. Catal., A 404 (2011) 103–112.
- [19] Y. Xiang, L. Ma, C. Lu, Q. Zhang, X. Li, Green Chem. 10 (2008) 939–943.
- [20] X. Yang, X. Yu, L. Long, T. Wang, L. Ma, L. Wu, Y. Bai, X. Li, S. Liao, Chem. Commun. 50 (2014) 2794–2796.
- [21] S.-I. Fujita, T. Yamada, Y. Akiyama, H. Cheng, F. Zhao, M. Arai, J. Supercrit. Fluids 54 (2010) 190–201.
- [22] F. Martínez-Espinar, P. Blondeau, P. Nolis, B. Chaudret, C. Claver, S. Castillón, C. Godard, J. Catal. 354 (2017) 113–127.
- [23] C.V. Rode, U.D. Joshi, O. Sato, M. Shirai, Chem. Commun. (2003) 1960–1961.
- [24] X. Yang, L. Du, S. Liao, Y. Li, H. Song, Catal. Commun. 17 (2012) 29–33.
- [25] H. Li, J. Liu, H. Li, Mater. Lett. 62 (2008) 297–300.
- [26] N.C. Nelson, J.S.N. Manzano, A.D. Sadow, S.H. Overbury, I.I. Slowing, ACS Catal. 5 (2015) 2051–2061.
- [27] G. Xu, J. Guo, Y. Zhang, Y. Fu, J. Chen, L. Ma, Q. Guo, ChemCatChem 7 (2015) 2485–2492.
- [28] H.-F. Li, Q.-S. Zhang, Z.-B. Pang, M. Tian, P. Gao, L.-L. Wang, Chin. Chem. Lett. 27 (2016) 1500–1504.
- [29] S. Ding, C. Zhang, Y. Liu, H. Jiang, R. Chen, Appl. Surf. Sci. 425 (2017) 484–491.
- [30] H. Zhou, B. Han, T. Liu, X. Zhong, G. Zhuang, J. Wang, Green Chem. 19 (2017) 3585–3594.
- [31] J.-F. Zhu, G.-H. Tao, H.-Y. Liu, L. He, Q.-H. Sun, H.-C. Liu, Green Chem. 16 (2014) 2664–2669.
- [32] Y. Li, X. Xu, P. Zhang, Y. Gong, H. Li, Y. Wang, RSC Adv. 3 (2013) 10973–10982.
- [33] C.-J. Lin, S.-H. Huang, N.-C. Lai, C.-M. Yang, ACS Catal. 5 (2015) 4121–4129.
- [34] F. Valentini, N. Santillo, C. Petrucci, D. Lanari, E. Petricci, M. Taddei, L. Vaccaro, ChemCatChem 10 (2018) 1277–1281.
- [35] R.D. Patil, Y. Sasson, Appl. Catal., A 499 (2015) 227–231.
- [36] D. Zhang, F. Ye, T. Xue, Y. Guan, Y.M. Wang, Catal. Today 234 (2014) 133–138.
- [37] V. Mévellec, A. Nowicki, A. Roucoux, C. Dujardin, P. Granger, E. Payen, K. Philippot, New J. Chem. 30 (2006) 1214–1219.
- [38] S. Nishimura, Handbook of Heterogeneous Catalytic Hydrogenation for Organic Synthesis, Wiley, New York, 2001.
- [39] S. Fehn, M. Zaheer, C.E. Denner, M. Friedrich, R. Kempe, New J. Chem. 40 (2016) 9252–9256.
- [40] I.E. Ertas, M. Gulcan, A. Bulut, M. Yurderi, M. Zahmakiran, J. Mol. Catal. A: Chem. 410 (2015) 209–220.
- [41] S. Kuklin, A. Maximov, A. Zolotukhina, E. Karakhanov, Catal. Commun. 73 (2016) 63–68.
- [42] P. Rasband, W. Hecker, J. Catal. 139 (1993) 551–560.
- [43] A. Abad, A. Corma, H. García, Chem. Eur. J. 14 (2008) 212–222.
- [44] R.E. Benfield, J. Chem. Soc., Faraday Trans. 88 (1992) 1107–1110.
- [45] R. Van Hardeveld, F. Hartog, Surf. Sci. 15 (1969) 189–230.
- [46] J.A. Anderson, F. Solymosi, J. Chem. Soc., Faraday Trans. 87 (1991) 3435–3442.
- [47] R. Cavanagh, J.T. Yates Jr, J. Chem. Phys. 74 (1981) 4150–4155.
- [48] J. Yates Jr, T. Duncan, S. Worley, R. Vaughan, J. Chem. Phys. 70 (1979) 1219–1224.
- [49] S. Trautmann, M. Baerns, J. Catal. 150 (1994) 335–344.
- [50] M.L. Honkela, J. Björk, M. Persson, Phys. Chem. Chem. Phys. 14 (2012) 5849–5854.
- [51] G. Li, J. Han, H. Wang, X. Zhu, Q. Ge, ACS Catal. 5 (2015) 2009–2016.

- [52] G. Kresse, J. Furthmüller, *Phys. Rev. B* 54 (1996) 11169.
- [53] G. Kresse, J. Furthmüller, *Comput. Mater. Sci.* 6 (1996) 15–50.
- [54] J.P. Perdew, K. Burke, M. Ernzerhof, *Phys. Rev. Lett.* 77 (1996) 3865.
- [55] S. Grimme, S. Ehrlich, L. Goerigk, *J. Comput. Chem.* 32 (2011) 1456–1465.
- [56] S. Grimme, J. Antony, S. Ehrlich, H. Krieg, *J. Chem. Phys.* 132 (2010) 154104.
- [57] G. Henkelman, B.P. Uberuaga, H. Jónsson, *J. Chem. Phys.* 113 (2000) 9901–9904.
- [58] D.J. Snelders, N. Yan, W. Gan, G. Laurenczy, P.J. Dyson, *ACS Catal.* 2 (2012) 201–207.
- [59] E. Finocchio, E. Macis, R. Raiteri, G. Busca, *Langmuir* 23 (2007) 2505–2509.
- [60] R. Duarte, O. Safonova, F. Krumeich, J. van Bokhoven, *Phys. Chem. Chem. Phys.* 16 (2014) 26553–26560.
- [61] J.F. Moulder, J. Chastain, *Handbook of X-ray Photoelectron Spectroscopy: A Reference Book of Standard Spectra for Identification and Interpretation of XPS Data*, Physical Electronics, 1995.
- [62] Y. Okamoto, N. Ishida, T. Imanaka, S. Teranishi, *J. Catal.* 58 (1979) 82–94.
- [63] J. Contour, G. Mouvier, M. Hoogewys, C. Leclere, *J. Catal.* 48 (1977) 217–228.